Optical Materials 58 (2016) 61–66

Contents lists available at ScienceDirect

Optical Materials

journal homepage: www.elsevier.com/locate/optmat

Ti:Sapphire micro-structures by femtosecond laser inscription: Guiding and luminescence properties

Yingying Ren [a, b, *], Yang Jiao [a], Javier R. Vázquez de Aldana [c], Feng Chen [b]

[a] School of Physics and Electronics, Shandong Normal University, Jinan 250014, China
[b] School of Physics, State Key Laboratory of Crystal Materials and Key Laboratory of Particle Physics and Particle Irradiation (MOE), Shandong University, Jinan 250100, China
[c] Laser Microprocessing Group, Universidad de Salamanca, Salamanca 37008, Spain

ARTICLE INFO

Article history:
Received 1 April 2016
Received in revised form
28 April 2016
Accepted 11 May 2016
Available online 19 May 2016

Keywords:
Optical cladding waveguides
Femtosecond laser micromachining
Ti:Sapphire crystal
Luminescence

ABSTRACT

We report on the fabrication of buried cladding waveguides with different diameters in a Ti:Sapphire crystal by femtosecond laser inscription. The propagation properties are studied, showing that the cladding waveguides could support near- to mid-infrared waveguiding at both TE and TM polarizations. Confocal micro-photoluminescence experiments reveal that the original fluorescence properties in the waveguide region are very well preserved, while it suffers from a strong quenching at the centers of laser induced filaments. Broadband waveguide fluorescence emissions with high efficiency are realized, indicating the application of the cladding waveguides in Ti:Sapphire as compact broadband luminescence sources in biomedical fields.

1. Introduction

In recent years, femtosecond laser inscription (FLI) has emerged to be a powerful micromachining technology in transparent dielectrics for the development of active integrated optical devices [1–3]. In crystalline materials and transparent ceramics, a negative refractive index (RI) change could be created in the exposed areas with certain fabrication conditions, and a RI increment caused by the lattice strain would be induced simultaneously in the vicinity of inscribed filaments. Channel waveguides compose of a pair of laser damage lines (with a separation of tens of micrometers) that can confine the light in the interline area or a single line guiding adjacent to the upper and lower tips of the filament have been fabricated by FLI [4,5]. More recently, depressed cladding waveguides have received increasing attention owing to their advantages. A circular cladding waveguide, with tube-like morphology, is composed of an unexposed material core surrounded by a large number of FLI induced low-index parallel tracks serving as waveguide boundaries. Such a structure has been fabricated in various optical crystals and transparent ceramics with lasers or nonlinear effects realized within the waveguides [6–11]. The diameter of cladding waveguides can be tailored with different inscription parameters to theoretically produce any sizes and shape of the waveguide cross section. Typically, the cross-sectional diameter is from 30 μm to 150 μm. A very unique feature of these flexible waveguide cores is that they enable the guidance from single-mode to highly multi-mode with visible to mid-IR wavelength regions [6,10]. In addition, the tubular structures of cladding waveguides offer the opportunity of 2D guidance along both TE and TM polarizations, which are almost identical in some crystals, making them ideal platforms for unpolarized pumping as light sources. Furthermore, the circular end-faces of cladding waveguides allow good connection with the commercial fibers, which also makes them advantageous in integrated photonics [4].

As an established material, Ti:sapphire (Ti^{3+}:Al_2O_3) has been proved to be one of the most attractive gain media with large gain bandwidth from ~600 nm to ~1000 nm [12]. The broadband fluorescence from Ti:Sapphire could be used in the biomedical field for, such as, optical coherence tomography (OCT), since the longitudinal resolution can be significantly improved with wide-spectrum sources [13]. However, the applications of bulk Ti:Sapphire could be frustrated, to certain extent, by relatively low light energy density as well as low compactness. Building waveguides in Ti:Sapphire samples could be a possible remedy to this

* Corresponding author. School of Physics and Electronics, Shandong Normal University, Jinan 250014, China.
E-mail address: ryywly@sdnu.edu.cn (Y. Ren).

http://dx.doi.org/10.1016/j.optmat.2016.05.023
0925-3467/

circumstance. Waveguide structures can confine the light beam in small volumes with the range of microns, leading to high intracavity light energy [14]. Waveguides with channel geometries, in particular, could provide confinement in two dimensions, which allow easy integration with other optical devices or circuits (e.g. OCT fiber-optic interferometric arrangements) and ensure high coupling efficiency. Additionally, larger fraction of fluorescence emission generated from waveguide structures could be collected through fundamental output modes, which would make Ti:Sapphire waveguides to be of much practical use as broadband fluorescence sources [15]. A number of research efforts have been dedicated to fabricating channel waveguides with single- or double-line structure in Ti:Sapphire via ultrafast laser inscription [16–19]. The fluorescence emission from single-line channel waveguides was reported, with slope efficiencies of the order of 10^{-5} [16]. Waveguide lasers from double-line structures were previously reported in Refs. [18] and [19]. However, remarkable polarization dependence was observed and only π polarized laser oscillations were achieved from these waveguides.

Since the emergence of the mid-infrared (MIR) laser sources, light in the MIR spectral band has been very attractive as it contains strong characteristic vibrational transitions of many important molecules and two atmospheric transmission windows (3–5 μm and 8–13 μm), which makes it crucial for applications in optical sensing, spectroscopy, thermal imaging, biomedicine, free-space communications. Ti:Sapphire crystal is one of the most promising materials for using in MIR region since it possesses high transmittance at around 3 μm–5 μm. Based on the waveguide geometries, some applications could be realized with integrated systems in chip-scale wafers. As of yet, there has no report on the characterizations of Ti:Sapphire waveguide structures at mid-infrared wavelengths.

In this work, we demonstrate depressed cladding waveguides in Ti:Sapphire fabricated by using FLI. Waveguiding performances (under 800 nm or 4 μm wavelength) and confocal microphotoluminescence properties of the cladding structures were investigated. The waveguides were further pumped by a 532 nm continuous-wave laser, producing a guided broadband fluorescence with power levels one order of magnitude larger than that of femtosecond-irradiation-induced channel waveguides previously reported [16].

2. Experimental procedures

High quality Ti:Sapphire crystal free of light scatter and with dislocation density less than 10^2 cm^{-2} was grown with Temperature Gradient Technique (TGT). The substrate, contained approximately 0.15 wt% Ti_2O_3, was cut into a dimension of 10(a) × 2(b) × 5(c) mm^3 and polished to optical quality.

2.1. Waveguide fabrication by FLI

Tubular cladding structures with three different diameters were produced along the a-axis inside the sample, as schematized in Fig. 1(a), in the laser facility of the Universidad de Salamanca. The procedure of waveguide writing is based on a Ti:Sapphire laser system (Spitfire, Spectra Physics, USA), which provides ultra-short pulses at 1 kHz repetition rate, with a pulse duration of 120 fs and a center wavelength of 795 nm. The laser beam was focused through a 20 × microscope objective (N.A. ~0.4) into the substrate at certain depth beneath one of the 5 × 10 mm^2 surfaces. The pulse energy incident on the sample was reduced to 1.7 μJ by utilizing a calibrated neutral density filter placed after a set of half-wave plate and a linear polarizer. Under our experimental conditions, this pulse energy was slightly over threshold to produce severe damage on the sample. In order to minimize the stress induced on the sample during irradiation, a large scanning velocity of 500 μm/s was chosen, that is small enough to ensure a good overlap between consecutive pulses. Then, while the substrate was translated perpendicularly to the laser beam axis at that speed, a set of parallel tracks (single scans) were inscribed at different depths of the sample (with ~230 μm being the maximum focusing depth) following the desired tubular geometry, from the bottom to the top. The lateral separation between adjacent scans was set to 3 μm in order to construct quasi-continuous boundaries, and the diameters of three cladding structures were 30 μm (WG1, composed of 24 tracks), 150 μm (WG2, composed of 106 tracks) and 100 μm (WG3, composed of 72 tracks), respectively. The fabrication time for the largest waveguide (WG2) took around 38 min.

2.2. Optical waveguide characterization

The guiding properties of these cladding structures at near-infrared (IR) or mid-IR wavelengths were experimentally characterized with typical end-face coupling arrangements, while half-wave plates were employed to control the polarization of the incident lasers to investigate the wave-guiding behaviors in both polarizations. In order to estimate the refractive index (RI) contrast Δn of waveguiding core with respect to the cladding area at MIR wavelength, a tuneable laser at 4 μm (MIR™ 8025, Daylight Solution Inc.) was employed as a light source, which was focused and then coupled into the waveguides by a MIR microscope objective lens (ZnSe, LFO-5-12-3.75, N.A. = 0.13). A MIR CCD camera (WinCamD-FIR-HR, DataRay Inc.) was utilized to map the near-field modal profiles of the cladding waveguide structures. By adjusting the position of the incident coupled light, the N.A. of the waveguide could be measured. The RI contrast was roughly approximated by using the formula [21]:

$$\Delta n = \frac{sin^2\theta_m}{n}$$

in which is the maximum incident angle where no change of the transmitted power is occurring, is the RI of Ti:Sapphire substrate. Further investigation about the waveguide losses under 800 nm was performed with a cw Ti:Sapphire laser (Coherent MBR PE, USA)

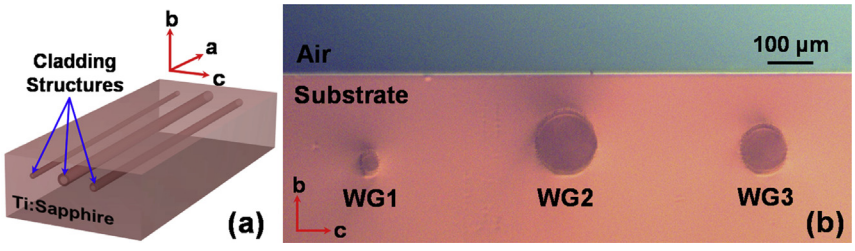

Fig. 1. (a) The schematic diagram of the Ti:Sapphire substrate with three cladding waveguides embedded below the surface, and (b) the cross sections of the cladding structures WG1, WG2 and WG3 in Ti:Sapphire fabricated by using FLI.

by detecting the incident and output beam power with a photodiode power sensor (Thorlabs S140C) while taking the Fresnel reflection of the end facets and the coupling efficiency into account, as previously introduced in Ref. [6]. The propagation loss α could be estimated by the equation:

$$P_{out} = P_{in} \cdot (1 - R)^2 \cdot e^{-\alpha L} \cdot \eta$$

where R is the Fresnel reflection coefficient, L denotes the length of the waveguide and η is the coupling losses caused by the mismatch between the pump beam mode and waveguide mode. In the mean time, the near-field modal profiles of the cladding waveguides under 800 nm were detected with NIR CMOS camera (CinCam CMOS 1201, Cinogy Technologies).

2.3. Confocal micro-luminescence measurements

Further investigations on the room-temperature confocal micro-photoluminescence (μ-PL) properties of the Ti:Sapphire cladding waveguides were performed with a fiber-coupled confocal microscope (Olympus BX-41). In this configuration, the 488 nm laser radiation from an argon laser was focused on the cross section by using an oil immersion 100 × microscope objective with N.A. = 0.95, exciting the transition of Ti^{3+} ions from their ground state $^2T_2$ up to ^2E excited state. The subsequent ^2E to $^2T_2$ fluorescence emission was then back-collected with the same microscope objective and, after passing through a series of filters and a confocal pinhole, analyzed by a high resolution fiber coupled spectrometer (SPE×500 M, USA). The sample was mounted to an XY motorized stage with a high spatial resolution of 100 nm so that the excitation spot could be scanned continuously over the waveguide's cross section.

2.4. Waveguide luminescence characterization

For waveguide luminescence characterization experiments, a cw laser (Verdi V8) generating a linearly polarized beam at 532 nm was employed as the pump source, in combination with a half-wave plate as well as an end-face pumping system. The pump laser beam was focused and coupled into the waveguide by using a spherical convex lens with a focal length of 75 mm, which gave a calculated diffraction limited spot size (diameter) of about 35 μm at the focus. The generated output beam was collected by a 20 × microscope objective (N.A. = 0.4). A dielectric mirror with high transmission at around 532 nm and high reflectivity at near-IR was butt-coupled to the input facet in order to increase the pump power launched into the waveguide and, at the same time, to back-reflect the counter-propagating luminescence which contributes to the output power. After being separated from the residual pump with a filter, the guided infrared fluorescence emission from the waveguide was detected. During the experiments, fluorescence properties in both of the two polarizations were investigated.

3. Results and discussion

Fig. 1(b) presents the cross sectional microscope images of the waveguides. As can be clearly seen, these structures were deeply embedded inside the Ti:Sapphire sample. The circularly-shaped waveguide boundaries were produced without any evident damage either in the waveguiding core areas or in the bulk outside the claddings.

Fig. 2(a)–(f) depict the experimental results for the near-field intensity (normalized) distributions of the Ti:Sapphire cladding waveguides at near-IR wavelength of 800 nm (Fig. 2(a)–(c)) and mid-IR wavelength of 4 μm (Fig. 2(d)–(f)). The guiding mode profiles shown in Fig. 2 were obtained under TE polarized (π polarized, i.e. the electric field was parallel to c-axis) pump beams. It should be pointed out that three waveguides could support both TE and TM polarizations, and the mode distributions did not exhibited significant polarization dependence as a result of symmetric morphology of the cladding structures. Strong optical confinement at 800 nm can be seen from Fig. 2(a)–(c), and the output beams at this wavelength possessed highly multi-mode profiles for all three waveguides. The mode numbers were reduced along with the reduction of the waveguide's diameters, implying that single-mode guidance could be expected with even smaller structure. Also, as shown in Fig. 2(d)–(f), the number of propagation modes was significantly decreased when pumping the waveguides with longer wavelength. WG1 was found to support single-mode guidance at 4 μm. In contrast, for WG2 and WG3, multi-mode guidance was achieved due to their relatively large size. The refractive index contrast of ~3×10^{-4} at 4 μm wavelength was obtained for single-mode waveguide WG1 under two transverse polarizations. Here, to simplify the RI profile model, a step-index configuration was assumed with a constant RI in each laser-induced filament, while the mechanical stress produced by ULI around the inscribed tracks was ignored since it decayed rapidly and had negligible influence on the waveguide modes [22]. The maximum values of propagation losses of the three waveguides under 800 nm were estimated to be around 5.8 dB/cm for WG1, 1.1 dB/cm for WG2 and 3.4 dB/cm for WG3, respectively, with a slight difference (around ±0.1 dB/cm) for TE and TM polarizations.

Fig. 3(a) illustrates the 1D integrated intensity profile of the Ti^{3+} emission line measured along the scan line crossing the center of WG2, while Fig. 3(b) are μ-PL emission spectra from the waveguide area, the filament and the unmodified bulk region corresponding to the red, blue and green spots in the inset. It can be observed from Fig. 3(a) that the μ-PL intensity increased at both sides of the damage tracks, while, at the centers of these damage tracks, it suffered from a strong quenching. The interpretation of these observations is not easy as the other fluorescence features (such as bandwidth or the spectral position) are not modified, as depicted in Fig. 3(b). Following previous works on other crystals (Nd:YAG for instance [23]), we correlated the strong fluorescence quenching at the track centers to the existence of a heavily doped damage core. It has been proved that the local lattice damage can lead to a reduction in the refractive index which can therefore act as a low-index cladding. The observed fluorescence increase at both sides of the damage tracks could be due to different reasons including lattice densification (that could lead to a local enhancement in the density of Ti emitting centers) or to an increment in the collection efficiency due to waveguiding effects caused by stress induced refractive index increments in the surroundings of the damage tracks. However, the precise reasons leading to the change of μ-PL intensity need to be further investigated. In any case data included in Fig. 3(a) demonstrate that in the active volume of the waveguide the Ti fluorescence was not deteriorated in respect to bulk due to the femtosecond inscription procedure, showing the potential of luminescence or laser emissions. Further evidence can be found from Fig. 3(b), in which a clear reduction of μ-PL intensity in the modified filament was occurred, while both spectra from waveguide and bulk were very similar without any variance of spectral distribution and intensity. These facts indicate that the mechanism leading to waveguide formation is the refractive index decrement created at filaments in company with the unmodified core areas.

Fig. 4 and 5 show the experimental results of the guided fluorescence characterizations from Ti:Sapphire cladding waveguides. The intensity profiles of the output signal originated from WG1, WG2 and WG3 under the excitation of a TE polarized pump laser at 532 nm are shown in Fig. 4(a)–(c). Transmission modes that covers

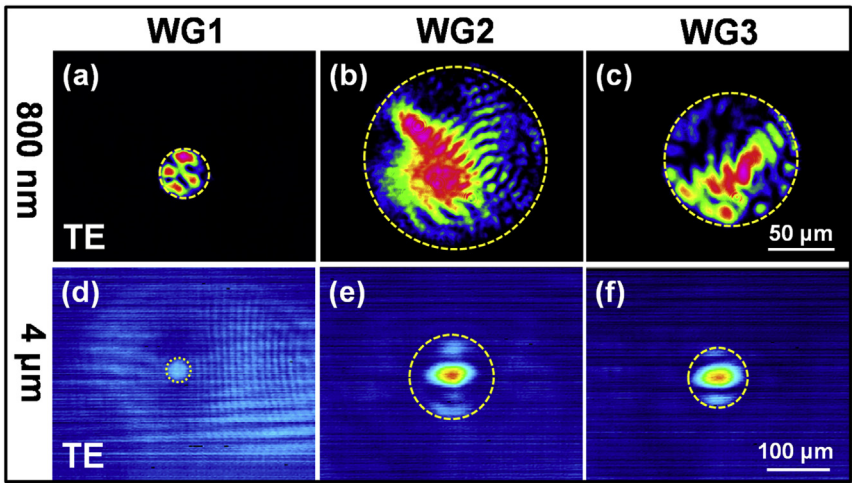

Fig. 2. Experimental mode intensity distributions from WG1, WG2 and WG3 at 800 nm (a–c) and 4 μm (d–f) at TE polarization. The yellow circles are the boundaries of the guiding areas. (For interpretation of the references to colour in this figure legend, the reader is referred to the web version of this article.)

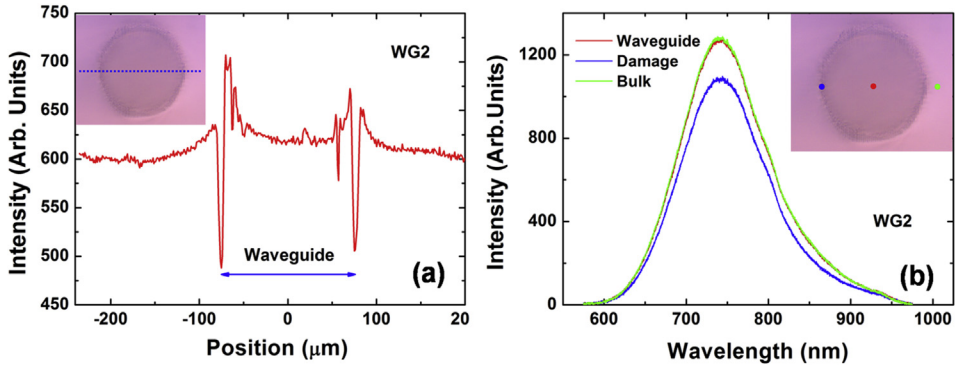

Fig. 3. (a) 1D distribution of the integrated μ-PL intensity; (b) comparison of the μ-PL spectra obtained from the waveguide area (red), the filament (blue) and the bulk (green). The insets show the cross section of the cladding waveguide WG2 and the scan line or spots. (For interpretation of the references to colour in this figure legend, the reader is referred to the web version of this article.)

all the waveguide's volumes was observed, showing a dramatic difference when compared with Fig. 2(a)–(c) which are the modal profiles of the three waveguides for an input laser light of 800 nm. This can be mainly attributed to the isotropy of the fluorescence signal of the corresponding spontaneous emission of Ti^{3+} ions. Similar modal distributions were experimentally obtained with a TM polarized pump beam, as can be confirmed from Fig. 4(d)–(f). The strong optical confinement of the fluorescence emission, which is more evident for WG2, could ensure efficient coupling to the fiber-optic interferometric arrangements used in OCT system.

Fig. 5(a) and (b) plot the curves of fluorescence output power as a function of incident power at 532 nm. It can be found that the

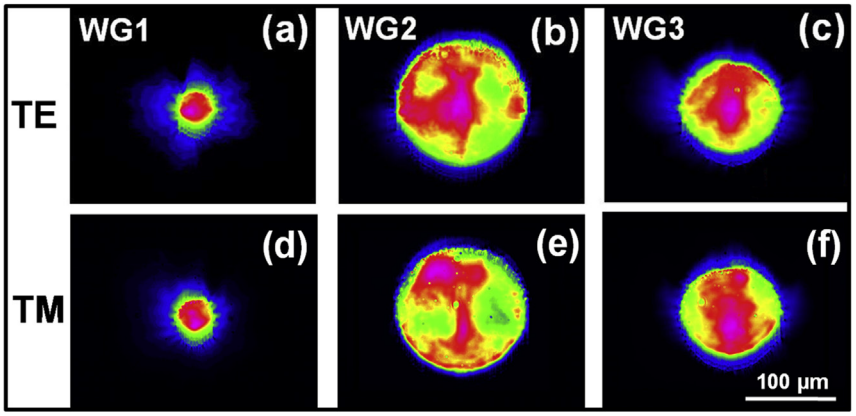

Fig. 4. Near-field intensity distribution of waveguide fluorescence from WG1, WG2 and WG3 under TE ((a)–(c)) and TM ((d)–(f)) polarized 532 nm pump.

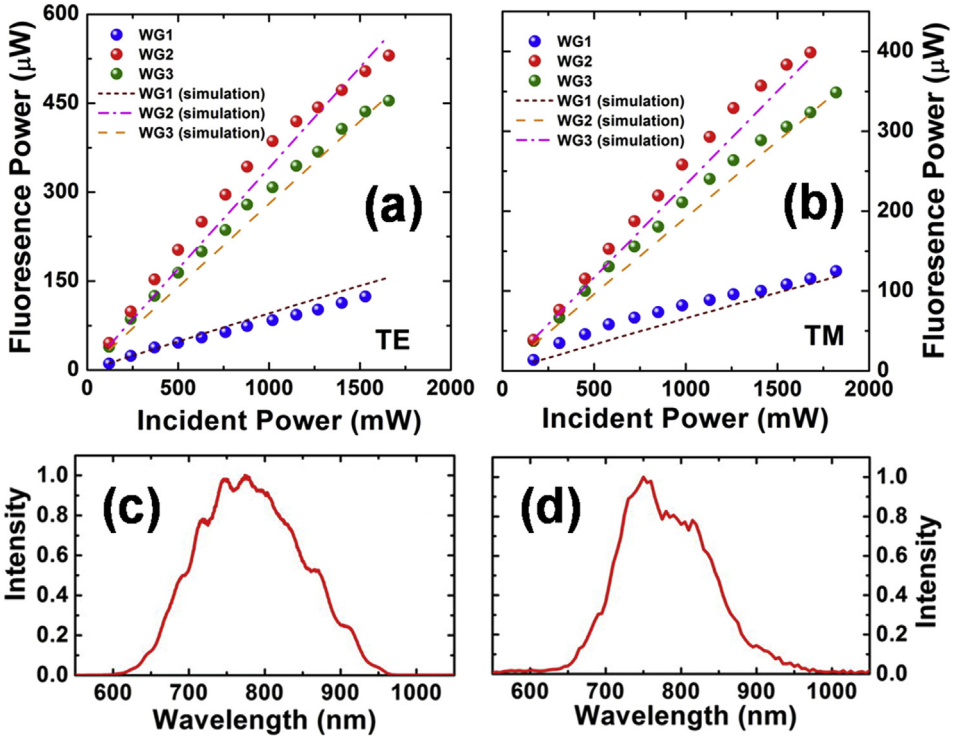

Fig. 5. Waveguide fluorescence power as a function of the incident power with TE (a) and TM (b) polarization. The lines refer to the calculated fluorescence output for WG1 (the dotted line), WG2 (the dashed line) and WG3 (the dashdotted line). (c) and (d) are fluorescence spectra.

fluorescence performances improved with increasing core diameters due to the reduction of the propagation losses, and the better performances were observed under π-polarization due to the larger absorption cross section. Among three waveguides, WG2 showed the highest output power up to 531 μW and 399 μW at 1660 mW (TE) and 1680 mW (TM) pumping, respectively, corresponding to a slope efficiency of 3.5×10^{-4} and 2.5×10^{-4}. WG3 gave a slope efficiency of 2.9×10^{-4} under TE polarization and a lower one of 2.0×10^{-4} under TM polarization. For WG1, the cladding waveguide with the smallest diameter, the slope efficiencies were further reduced to 0.8×10^{-4} and 0.7×10^{-4} at TE and TM polarized pump beams. These values of the slope efficiency for fluorescence emission in our work have an order of magnitude improvement compared with those recorded from the stress induced channel waveguide in Ti:Sapphire fabricated by femtosecond laser writing, as reported in Ref. [16]. Additionally, the waveguides fabricated in this work are more advantageous for fluorescence radiation under both orthogonal polarizations, while guiding effects with a certain polarization were found from femtosecond laser inscribed double-line Ti:Sapphire waveguides [18,19]. The curvature of the experimental results could be attributed to saturation of the absorption in the guiding areas. To estimate the theoretical fluorescence output power as a function of the input power and the waveguide size under different polarizations, we followed the four-level system model and calculation methods as outlined in Ref. [20]. The lines in Fig. 5(a) and (b) represent the calculated fluorescence power as a function of pump power for cladding structures with various diameters as well as different pumping polarizations. It can be observed that the theoretical fluorescence powers are in good agreement with the experimental results. Fig. 5(c) and (d) depict the fluorescence spectra achieved at TE and TM polarization with a broad bandwidth (FWHM) of ~180 nm and ~140 nm, respectively.

4. Conclusion

In conclusion, we have presented a study of the waveguiding and luminescence features of Ti:Sapphire cladding waveguides fabricated by FLI. The fabricated structures were capable of supporting orthogonal polarizations in a wide spectral range up to 4 μm without any deterioration in the fluorescence properties of Ti^{3+} ions in the waveguide areas. Broadband waveguide fluorescence emissions were realized with a maximum slope efficiency of 3.5×10^{-4}, beating the previously reported performances of femtosecond laser inscribed waveguide fluorescence [16] by an order of magnitude. The good performances of these depressed-cladding structures make them suitable luminescence sources in integrated optical circuits for the biomedical application (such as optical coherence tomography). In addition, these cladding waveguides also show their potential for tunable waveguide laser generation without any pumping polarization dependence, which will be confirmed experimentally in our future works.

Acknowledgements

This work was supported by the National Natural Science Foundation of China (No. 11404194 and No. 11274203) and Junta de Castilla y León (Project SA086A12-2). J. Yang acknowledges the support from the National Natural Science Foundation of China (No. 11405098). The authors thank D. Jaque for μ-PL measurement of the sample.

References

[1] R.R. Gattass, E. Mazur, Femtosecond laser micromachining in transparent materials, Nat. Photonics 2 (2008) 219–225.
[2] M. Ams, G.D. Marshall, P. Dekker, J.A. Piper, M.J. Withford, Ultrafast laser written active devices, Laser Phot. Rev. 3 (2009) 535–544.
[3] K. Sugioka, Y. Cheng, Ultrafast lasers-reliable tools for advanced materials

processing, Light Sci. Appl. 3 (2014) e149.
[4] F. Chen, J.R. Vázquez de Aldana, Optical waveguides in crystalline dielectric materials produced by femtosecond-laser micromachining, Laser Photonics Rev. 8 (2014) 251–275.
[5] J. Burghoff, S. Nolte, A. Tünnermann, Origins of waveguiding in femtosecond laser-structured $LiNbO_3$, Appl. Phys. A 89 (2007) 127–132.
[6] Y.Y. Ren, J.R. Vázquez de Aldana, F. Chen, H.J. Zhang, Channel waveguide lasers in Nd:LGS crystals, Opt. Express 21 (2013) 6503–6508.
[7] N. Pavel, G. Salamu, F. Voicu, F. Jipa, M. Zamfirescu, T. Dascalu, Efficient laser emission in diode-pumped Nd:YAG buried waveguides realized by direct femtosecond-laser writing, Laser Phys. Lett. 10 (2013) 195802.
[8] Y.Y. Ren, G. Brown, A. Ródenas, S. Beecher, F. Chen, A.K. Kar, Mid-infrared waveguide lasers in rare-earth doped YAG, Opt. Lett. 37 (2012) 3339–3341.
[9] G. Salamu, F. Jipa, M. Zamfirescu, N. Pavel, Cladding waveguides realized in Nd:YAG ceramic by direct femtosecond-laser writing with a helical movement technique, Opt. Mater. Express 4 (2014) 790–797.
[10] G. Salamu, F. Jipa, M. Zamfirescu, N. Pavel, Laser emission from diode-pumped Nd:YAG ceramic waveguide lasers realized by direct femtosecond-laser writing technique, Opt. Express 22 (2014) 5177–5182.
[11] N.N. Dong, F. Chen, J.R. Vazquez de Aldana, Efficient second harmonic generation by birefringent phase matching in femtosecond laser inscribed KTP cladding waveguides, Phys. Status Solidi R 6 (2012) 306–308.
[12] P.F. Moulton, Spectroscopic and laser characteristics of $Ti:Al_2O_3$, J. Opt. Soc. B 3 (1986) 125–133.
[13] A. Kowalevicz, T. Ko, I. Hartl, J.G. Fujimoto, M. Pollnau, R.P. Salathé, Ultrahigh resolution optical coherence tomography using a superluminescent light source, Opt. Express 10 (2002) 349–353.
[14] C. Grivas, Optically pumped planar waveguide lasers, Part I: fundamentals and fabrication techniques, Prog. Quantum Electron 35 (2011) 159–239.
[15] M. Pollnau, R.P. Salathé, T. Bhutta, D.P. Shepherd, R.W. Eason, Continuous-wave broadband emitter based on a transition-metal-ion-doped waveguide, Opt. Lett. 26 (2001) 283–285.
[16] V. Apostolopoulos, L. Laversenne, T. Colomb, C. Depeursinge, R.P. Salathe, M. Pollnau, R. Osellame, G. Cerullo, P. Laporta, Femtosecond-irradiation-induced refractive-index changes and channel waveguiding in bulk Ti^{3+}: Sapphire, Appl. Phys. Lett. 85 (2004) 1122–1124.
[17] J. Bai, G.H. Cheng, X.W. Long, Y.S. Wang, W. Zhao, G.F. Chen, R. Stoian, R.Q. Hui, Polarization behavior of femtosecond laser written optical waveguides in Ti: Sapphire, Opt. Express 20 (2012) 15035–15044.
[18] C. Grivas, C. Corbari, G. Brambilla, P.G. Lagoudakis, Tunable, continuous-wave Ti:sapphire channel waveguide lasers written by femtosecond and picosecond laser pulses, Opt. Lett. 37 (2012) 4630–4632.
[19] C. Grivas, C. Corbari, G. Brambilla, Recent Progress in Continuous-wave Ti: Sapphire Waveguide Lasers, Integrated Optics: Devices, Materials, and Technologies XVIII, 898808, 2014.
[20] C. Grivas, D.P. Shepherd, T.C. May-Smith, R.W. Eason, M. Pollnau, A. Crunteanu, M. Jelínek, Performance of Ar^+-Milled Ti:Sapphire Rib waveguides as single transverse-mode broadband fluorescence sources, IEEE J. Quantum Electron 39 (2003) 501–507.
[21] J. Siebenmorgen, K. Petermann, G. Huber, K. Rademaker, S. Nolte, A. Tünnermann, Femtosecond laser written stress-induced $Nd:Y_3Al_5O_{12}$ (Nd: YAG) channel waveguide laser, Appl. Phys. B 97 (2009) 251–255.
[22] A. Okhrimchuk, V. Mezentsev, A. Shestakov, I. Bennion, Low loss depressed cladding waveguide inscribed in YAG: Nd single crystal by femtosecond laser pulses, Opt. Express 20 (2012) 3832–3843.
[23] H.L. Liu, Y.C. Jia, J.R. Vázquez de Aldana, D. Jaque, F. Chen, Femtosecond laser inscribed cladding waveguides in Nd:YAG ceramics: fabrication, fluorescence imaging and laser performance, Opt. Express 20 (2012) 18620–18629.